Fluid Phase Equilibria 531 (2021) 112911

Contents lists available at ScienceDirect

Fluid Phase Equilibria

journal homepage: www.elsevier.com/locate/fluid

Wax precipitation modelling using Perturbed Chain Statistical Associating Fluid Theory (PC-SAFT)

I. Shahsenov[a,*], I. Baghishov[b], P. Allahverdiyev[c], E. Azizov[c]

[a] Khazar University eiLink R&D Center, Baku, AZ1005, Azerbaijan
[b] The University of Texas at Austin, petroleum and geosystems engineering department, Austin, Texas, 78712, USA
[c] BP AGT, Reservoir Development BP Azerbaijan, Baku, AZ1005, Azerbaijan

ARTICLE INFO

Article history:
Received 20 May 2020
Revised 19 November 2020
Accepted 22 November 2020
Available online 26 November 2020

Keywords:
Flow assurance
Wax precipitation modelling
PC-SAFT
Heat equation
Calibration of EOS

ABSTRACT

Wax precipitation is one of the most challenging flow assurance problems because of its ability to create restrictions to flow inside wellbores, pipelines, and some production facilities. Inaccuracy in predictions of wax appearance temperature (WAT) and amount of precipitated wax makes it necessary to reassess existing thermodynamic models. In addition, most of the current models require accurate description of wax composition from expensive PNA analysis.

Here we propose to substitute traditional cubic equations-of-state with Perturbed Chain form of the Statistical Associating Fluid Theory (PC-SAFT). The advantage of PC-SAFT is mainly the accuracy in the estimation of fugacities of heavy components in vapor and liquid mixtures. These fugacities are important because they define the equilibrium between wax, liquid and vapor phases. The novelty of this research was in approach for fluid characterization. Such models as multi-solid or solution-solid were not used. Instead, wax phase was represented as one phase and its amount was taken from inexpensive cross-polarized microscopy data. Therefore, we did not need PNA analysis. To be able to accurately predict with one wax component, reservoir was divided into sectors to determine PC-SAFT parameters for this wax component from calibration of each sector separately. Later, when a new well is drilled, its content of wax can be determined from the cross-polarized experiment and PC-SAFT parameters are same as PC-SAFT parameters of that sector (they were obtained from calibration for that sector before). This data alone is enough to predict amount of precipitated wax at any conditions with high accuracy.

First, we validated PC-SAFT with experimental PVT data such as bubble point pressure, gas-to-oil ratio (GOR) and oil formation volume factor (Bo) and compared to the results of Peng Robinson EoS. This PVT data is from one of the fields in the South Caspian Basin. The first validation of wax precipitation itself, however, was performed on experimental data in the literature. Later, the model was calibrated on the oil sample data (composition and wax data from cross-polarized lab experiment) from the field in the South Caspian Basin. Finally, we verified the model with the data from the rest of the wells in this field. The results prove the accuracy of PC-SAFT method and show that costs of PNA analysis can be avoided if cross-polarized microscopy is available.

1. Introduction

Hydrocarbon mixtures travel a couple of kilometers from the reservoir all the way up to the surface through the tubing and then several kilometers more from the well to the surface facilities in pipelines which may be located under the sea. When hot fluid travels in the pipeline immersed in the water, it cools down which may cause such heavy hydrocarbons to precipitate out of the liquid as paraffins that form a wax. Even though a flowing oil through subsea pipelines is the commonplace of wax precipitation, it may accumulate during production in the tubing as well, especially in case if the wellbore is located in the long sea section. This precipitation of wax in the tubing is not always guaranteed as the temperature in the wellbore changes drastically depending on the flowrates and many other factors that may change from well to well. In addition to that, unpredicted precipitations of wax may cause a lot of troubles during intervention into the well. Therefore, correct identification of wells with a potential wax deposition before intervention into the well is one of the current requirements

* Corresponding author.
E-mail address: izat.shahsanov@khazar.org (I. Shahsenov).

https://doi.org/10.1016/j.fluid.2020.112911
0378-3812/

in the petroleum industry. Otherwise, equipment used during this process may get stuck in the wax deposits. Wax crystals in oil may also cause such problems as the increase of viscosity, leading to pressure losses and the requirement of higher yield stress for restarting the flow [1]. Thus, it is crucial to recognize wells with precipitated wax in order to correctly determine a stimulation procedure that should be performed to increase their oil rate. In addition, it is important to rank wells with high wax precipitation risk in order to address it during well entry plan to minimize potential NPT (Non-Productive Time). Therefore, a necessity in the accurate estimation of the amount of wax precipitated at certain conditions in the well and wax appearance temperature (WAT) arises.

Unfortunately, nowadays, models used in the industry overestimate the amount of precipitated wax and do not show a good match with the experimental data. Models can be classified into two parts: Multi Solid and Solution Solid Models which are used together with a cubic Equations of State (EOS).

The main assumption behind the Solution Solid (SS) Model is that all precipitating components are miscible with each other and create a solid solution (SS). A cubic EOS is used in this model for the calculation of fluid fugacities and defining vapor-liquid equilibrium (VLE). Solid-liquid equilibrium, however; is defined through an activity coefficient model. One of the most famous solid solution models for wax precipitation was proposed by Won [2,3] which used Soave-Redlich-Kwong EOS as a tool for VLE. The description of liquid on the liquid-solid coexistence curve was achieved through a modified regular solution theory. Hansen et al. [4] modified the activity coefficient of a liquid phase in a regular solution using the theory of multi-component polymer solutions proposed by Flory [5]. Pedersen et al. [6] improved the model proposed by Won [2] to calculate WAT. The model validation was performed with the experimental WAT data of oils from the North Sea. Coutinho and Stenby [7] described orthorhombic solid phases using Wilson's model, then Coutinho [8] improved the UNIQUAC model to describe the orthorhombic solid phase more accurately. Solid Solution model developed by Zuo et al. [9] considers the Poynting correction in the calculation of wax fugacity and is able to predict WAT over a wide range of wax content values and pressures. Ji et al. [10] applied the UNIQUAC thermodynamic model and achieved wax disappearance temperature prediction. First, the thermodynamic properties of n-paraffins were calculated, following that a new methodology based on the UNIQUAC model was described. Esmaeilzadeh et al. [11] examined different activity coefficient models on prediction of the behavior of the solid phase and validated Wilson's model using experimental data of binary, ternary, quaternary and multi-component fluids. Coutinho and Ruffier Meŕay [12] investigated the deposition of wax using both thermodynamic and experimental methods. Modeling of wax formation from hydrocarbon fluids was performed using the predictive UNIQUAC model.

The other category of available models for thermodynamic modeling of wax precipitation is Multiple Solid (MS) where precipitated solid phases are separate and are not miscible. MS model was presented by Lira-Galeana et al. [13] where wax solids were described as multi pure-solids. The Peng Robinson (PR) EOS was employed for liquid and vapor fugacity calculations. Vafaie Sefti et al. [14] utilized the MS model for predictions of the equilibrium phase in crude oil. PR EOS was used for the description of fluid properties. Dalirsefat and Feyzi [15] achieved predictions of WAT and the amount of wax precipitated using a modified MS model. Modification of PR EOS was used for the calculation of liquid and gas-phase fugacities.

In these methodologies, equilibrium is determined using a fugacity equality method where fugacity of solid phase is calculated from the fugacity ratio formula and fugacities in vapor and liquid mixtures are estimated using a cubic equation of state. Hence, it is crucial to have EOS that accurately calculates the fugacity of all components in liquid and vapor, especially of heavy components. Even though this methodology is widespread, cubic equations of state are some kind of Van der Waal's EOS modifications and the shape of the molecules was not considered which is a big assumption for components with high carbon numbers. Therefore, these EOS has some limitations and uncertainties when it comes to determining fugacities of components with the high carbon number which are particularly important for solid-liquid equilibrium. Even though such modification as critical parameters or adjustment of molecules non-sphericity in these EOS increased their accuracy, determining of these parameters for heavy components is nearly impossible as they degrade during the experiment when the temperature or pressure is increased to the critical.

This study proposes to use Perturbed Chain form of Statistical Associating Fluid Theory, PC-SAFT, instead of cubic equation of state due to its derivation procedure (derived from statistical mechanics) and molecules shape being represented in the form of chains of spherical segments which is the better imitation of major real molecules of heavy hydrocarbon [16]. Especially, this representation is close to the reality for wax molecules themselves as molecules precipitating in the form of wax are mainly straight-chain alkanes with very little branching. [1,17]. The reason for that phenomenon is that for the hydrocarbon it is easier to agglomerate into larger particles if they are long and straight rather if they are branched molecules with the same carbon number as the surface area of long and straight molecules is bigger [18].

Statistical Associating Fluid Theory was developed by Chapman, et al. [19] by extending and simplifying Wertheim's theory for associating fluids [20]. According to SAFT, the free energy of a fluid is determined by summing up the free energies of an aggregate of spherical segments and the free energy change spent on bonding of the segments in a structure that resembles the molecules of interest. Wertheim's theory is used to calculate that change in free energy. Various modifications of the SAFT have been proposed over the years. The only difference between these models is in segment term accounting for the Van der Waals attraction forces. All of the proposed forms of the SAFT EOS utilize chain and association terms that were originally described by Chapman, et al. Perturbed Chain form of SAFT (PC-SAFT) was developed by Gross and Sadowski [16] after extending the Barker and Henderson's [21] perturbation theory to a hardchain reference. PC-SAFT utilizes a hard-sphere reference fluid first described by EOS of Mansoori et al. [22]. This modification of SAFT allowed for proper predictions of the phase behavior of heavy molecules.

In this work, due to the lack of PNA analysis and availability of wax weight percentage from experiments, the methodology of representing wax in the composition as one component was applied. Owing to the characterization of precipitating wax as one component, there was no need for Multi Solid or Solution Solid model.

2. Methodology

In this section, we first explain our fluid characterization technique and then introduce the concepts of solution-solid and Multi-Solid Models. We then develop the underlying theory of how these models are used together with PC-SAFT Equation of State in the three-phase flash calculation algorithm.

2.1. Fluid characterization

Lack of PNA hindered our ability to characterize the composition of wax. However, wax weight % and wax appearance temperature (WAT) for all the wells from cross-polarized microscopy experiment was available to us. Moreover, compositions of oil from 12 wells spread across the reservoir was also accessible.

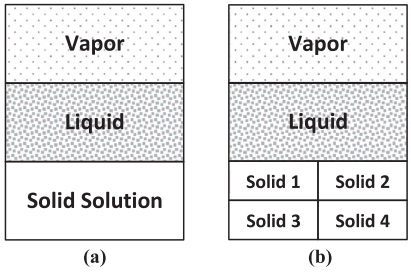

Fig. 1. (a) Solution solid model, (b) Multi-solid model.

Composition of wax is different across the field which makes it more difficult to predict wax precipitation if wax is represented as one component. Therefore, we need to have different PC-SAFT and fusion parameters for wells across the reservoir which limits the predicting capability. Hence, the methodology used in this paper is to group the wells with similar wax properties and calibrate every group of wells separately and obtain one set of PC-SAFT parameters for every group. If prediction of a new well is required in future, then the group to which this well belongs needs to be determined and this calibrated set of parameters of that group can be used.

By referring to compositional variation across the field and wax weight percentage along with WAT data, reservoir was divided into 5 sectors containing about 25–35 wells. One representative composition was selected for every sector from available compositional analysis data. As every well had wax weight percentage data, composition for every well can be calculated by substituting wax percentage and normalizing the composition. This fluid characterization technique was used to predict wells not used in the calibration procedure (more about this when Fig. 5 is described).

2.2. Solution solid and multi-solid models

Multi-Solid (MS) and Solution Solid (SS) models both are set of isofugacity conditions described to calculate the amount of precipitated solid phase. The difference between the models is the representation of the solid phase. In the latter case precipitating components are miscible with other solid components creating a solution of solids, however, in MS model the solid components are considered to form separate phases that do not mix with each other. These models are illustrated below in Fig. 1a and b.

In both models, fugacities of non-precipitating components in the vapor mixture will be equal to fugacities of the same components in the liquid mixture, as in the case of simple vapor liquid equilibrium. However, what differs in these models is the fugacity of precipitating components. Since solid components in the SS model are all dissolved in one solid solution, isofugacity condition for precipitating components (noted as i) will be as follows:

$$f_i^V = f_i^L = f_i^S \tag{1}$$

Where, f_i^π is fugacity of i component in π phase mixture. Fugacities in liquid or vapor mixtures can be calculated using equations of state (e.g. such cubic EOS as Peng-Robinson, Soave modification of Redlich Kwong). Fugacity of i component in the solid mixture, however, calculated using activity coefficient from pure solid fugacity:

$$f_i^S = x_i^S \gamma_i^S f_{pure,\ i}^S \tag{2}$$

Where, x_i^S is the composition and γ_i^S is the activity coefficient of i component in solid solution.

Fugacity of pure solid is calculated from the fugacity ratio formula [23]:

$$\ln\left(\frac{f_{pure,\ i}^S}{f_{pure,\ i}^L}\right) = \frac{\Delta h_i^f}{RT}\left(\frac{T}{T_i^f} - 1\right) - \frac{\Delta C_{pi}}{R}\left(1 - \frac{T_i^f}{T} + \ln\left(\frac{T_i^f}{T}\right)\right) \tag{3}$$

Fugacity of pure liquid ($f_{pure,\ i}^L$) can be determined from EOS. In the above formula, Δh_i^f is the fusion enthalpy, ΔC_{pi} is the difference between heat capacities of liquid and solid phases and T_i^f is the temperature of fusion.

On the other hand, precipitated components are forming separate solid phases according to the MS model. Therefore, the fugacity of i component in liquid or vapor mixture should be equal to pure fugacity of i component in solid-state. The formula is provided below:

$$f_i^V = f_i^L = f_{pure,\ i}^S \tag{4}$$

However, in this study, some components are lumped together. Therefore, the composition consists of 8 components (CO_2, C_1+N_2, C_2, C_3–C_4, C_5–C_{10}, C_{11}–C_{20}, $C_{21+\ \text{non-precip}}$, wax). The Component called "wax" is the precipitating part of C_{21+}. This type of characterization was used due to the absence of PNA analysis and the presence of experimental data for dissolved wax weight %. Therefore, the value of wax percentage is obtained from the experiments which were carried out on the samples from almost all the wells in the field. Since only one solid component is present, neither Multi-Solid nor Solution Solid Models were used.

The isofugacity condition for non-precipitating ***i*** and precipitating (wax) components implemented in this study are as follows:

$$f_i^V = f_i^L \tag{5}$$

$$f_{wax}^V = f_{wax}^L = f_{pure,\ wax}^S \tag{6}$$

Fugacities of all the components (including wax component) in the vapor and liquid mixtures are estimated by PC-SAFT. Pure solid fugacity of wax is calculated from Eq. (3) where fusion properties and fugacity of pure wax in liquid state are required. Fugacity of pure wax in liquid state is obtained from PC-SAFT. Fusion properties, required in Eq. (3) are calculated using correlations found from the literature and then all of these properties were tuned to match experimental data in the calibration process:

Fusion temperature of wax component was described using Chen's correlation [24]:

$$T_{wax}^f = 411.4 - \frac{32326}{MW_{wax}} \tag{7}$$

Won proposed this correlation of Enthalpy of fusion for paraffinic components [2]:

$$\Delta h_{wax}^f = 0.1426 MW_{wax} T_{wax}^f \tag{8}$$

Heat capacity change, however, calculated using correlation of Pedersen [6]:

$$\Delta C_{pwax}^f = 0.3033 MW_{wax} - 4.635 * 10^{-4} MW_{wax} T \tag{9}$$

2.3. Perturbed Chain Statistical Associating Fluid Theory (PC-SAFT)

PC-SAFT was derived with an application of the perturbation theory of Barker and Henderson to a hard-chain reference fluid. The authors of this equation of state claim that PC-SAFT is applicable to a wide range of fluids from mixtures with small spherical molecules, nonspherical solvents up to chainlike polymers.

Unlike cubic EOS, PC-SAFT was not derived with an assumption of sphericity of molecules. Molecules are represented in the form

of chains consisting of spherical segments, which makes it applicable to wax precipitation modeling. There are three main parameters of PC-SAFT required for each component in the composition: number of segments (m), segment diameter (σ) and the energy parameter (ε/k) [16].

In order to accurately predict the equilibrium between solid, vapor and liquid, it is crucial to determine fugacities precisely. The equation for calculating fugacity of pure solid phase derived analytically with small assumptions; however, this fugacity depends on the accuracy of fusion properties and fugacity of the same component in liquid state which is determined using the equation of state. Moreover, fugacities in liquid and vapor mixtures are derived from EOS. Hence, EOS accuracy is the principal factor in calculating the amount of precipitated wax. Hence, PC-SAFT is used instead of cubic EOS in this work.

First, after temperature, pressure, and composition are inputted into the algorithm, the Newton-Raphson Method determines the density of the fluid by converging to the pressure outputted by PC-SAFT. Following this, the fugacity of all components in vapor and liquid can be calculated using the density and PC-SAFT.

The block diagram of how PC-SAFT was used to calculate fugacity is provided in Appendix A. Equations required for calculation of fugacity are presented in Appendix B.

Previously mentioned fugacity ratio formula for defining solid-phase fugacity and PC-SAFT algorithm for calculating fugacity in a fluid mixture has to be used together in phase flash calculation to quantify amount of each phase. Owing to the presence of gas, oil and solid wax phases in the tubing, the three-phase flash calculation is utilized.

Inaccuracy in initial values of liquid and solid mole fractions and K value (Henry's law constant) can cause convergence problem that substantially increases the runtime. Therefore, two phase flash calculations (Vapor-Liquid and Liquid-Solid) are performed and their results are used to calculate the initial values.

The Block Diagram of Three Phase Flash Calculation is provided in Appendix A (Fig. A.2).

2.4. Radial temperature gradient inside the tubing

Property most affecting wax precipitation is known to be temperature. It was also illustrated in the sensitivity analysis graphs in the results section.

During this study, the temperature profile was obtained from Distributed Temperature Sensing (DTS) data. However, due to the location of fibre optic cable, temperature from DTS does not exactly represent the temperature of flowing fluids inside the tubing. Usually, the temperature of the oil in the flow center is hotter than DTS.

Therefore, the heat transfer equation was used to model the radial temperature gradient and therefore determine the temperature of oil flowing inside the tubing. Heat flow equation in radial coordinates is given below [25]:

$$\frac{\partial T}{\partial t}+\left(V_r\frac{\partial T}{\partial r}+V_\theta\frac{1}{r}\frac{\partial T}{\partial \theta}+V_z\frac{\partial T}{\partial z}\right) = (\varepsilon_h+\alpha_T)\left(\frac{1}{r}\frac{\partial}{\partial r}\left(r\frac{\partial T}{\partial r}\right)+\frac{1}{r^2}\frac{\partial^2 T}{\partial \theta^2}+\frac{\partial^2 T}{\partial z^2}\right)+R \tag{10}$$

Where V is velocity, T is temperature, ε_h is turbulent heat diffusivity, α_T is thermal diffusivity, R is generation term and r, θ, z are radial coordinates

During turbulent flow in the pipe, eddies and vortices result in local advection in all three directions. These localized advective motions sum up as a resultant diffusivity in the direction of temperature change of concentration. Therefore, advection is mainly substantial in the direction of flow (axial direction). Diffusion in the axial direction can be neglected since it is much smaller than transport due to advection. Since the purpose is to find a steady-state solution, the transient accumulation term can be ignored. After removing parts of the equation discussed above, the following equation is derived:

$$V_z\frac{\partial T}{\partial z}=(\varepsilon_h+\alpha_T)\frac{1}{r}\frac{\partial}{\partial r}\left(r\frac{\partial T}{\partial r}\right)+R \tag{11}$$

The generation terms that are left in Eq. (11) can be caused by crystallization in the fluid. During crystallization, process heat is gained and mass is lost out of fluid. According to Lee heat obtained from crystallization is less than 0.1% and negligible compared to diffusion and advection terms [26]. Thus, the generation term is also removed

After the rearrangement of the equation and replacing a sum of two diffusivity terms, $\varepsilon_h+\alpha_T$ with total diffusivity, α_{tot} following equation is derived:

$$V_z\frac{\partial T}{\partial z}=\alpha_{tot}\frac{\partial^2 T}{\partial r^2}+\frac{\alpha_{tot}}{r}\frac{\partial T}{\partial r} \tag{12}$$

Then, finite difference methodology was applied to the Eq. (12) and temperature was discretized in 2D space (radius and depth). As a result, the temperature in any location of the tubing was obtained.

One of the example outcomes of the simulation is provided in Fig. 2.

Here, color and vertical axis represent the temperature at a certain distance from the flow center and depth of the wellbore (in other words, tubing length). As a result of the simulation, depending on flowrates, the temperature in the center of the flow may be 2–4 °C higher than at the edges (or at DTS fiber). As the radius of the tubing was approximately 6 cm in Fig. 2, temperatures at the highest distance on the plot represent the DTS profile.

2.5. Calibration of model parameters on WAT prediction

As it was described in the Fluid Characterization section of this paper, the oil field was divided into sectors containing similar wax properties. This was done due to vast size of the field and variations in the composition which was making calibration and prediction of all the wells impossible as wax was represented as one component. Therefore, calibration was carried out on each group of wells (sector of the oil field) separately. About 30–40% of the wells were used for the calibration procedure and the rest of them were used for testing. The calibration methodology itself is described as follows.

Predictions of WAT depend on accurate determination of equilibrium point which in turn depends on fugacity calculations of all the phases. As liquid and gas phase fugacities are calculated using PC-SAFT and fugacity of solid phase is calculated from fugacity ratio formula, main parameters of PC-SAFT (m, σ and ε/k) and fugacity ratio formula (Δh_i^f, ΔC_{pi} and T_i^f) may be tuned to match the experimental values of WAT.

Gradient Descent optimization algorithm was used to automize the calibration procedure. General equation form of the optimization algorithm is given below:

$$x_{n+1}=x_n-\nabla F(x_n) \tag{13}$$

Where F is the residual sum of squares of model's WAT prediction and x is a parameter to be tuned (e.g. m, σ, ε/k, Δh_i^f, ΔC_{pi} and T_i^f).

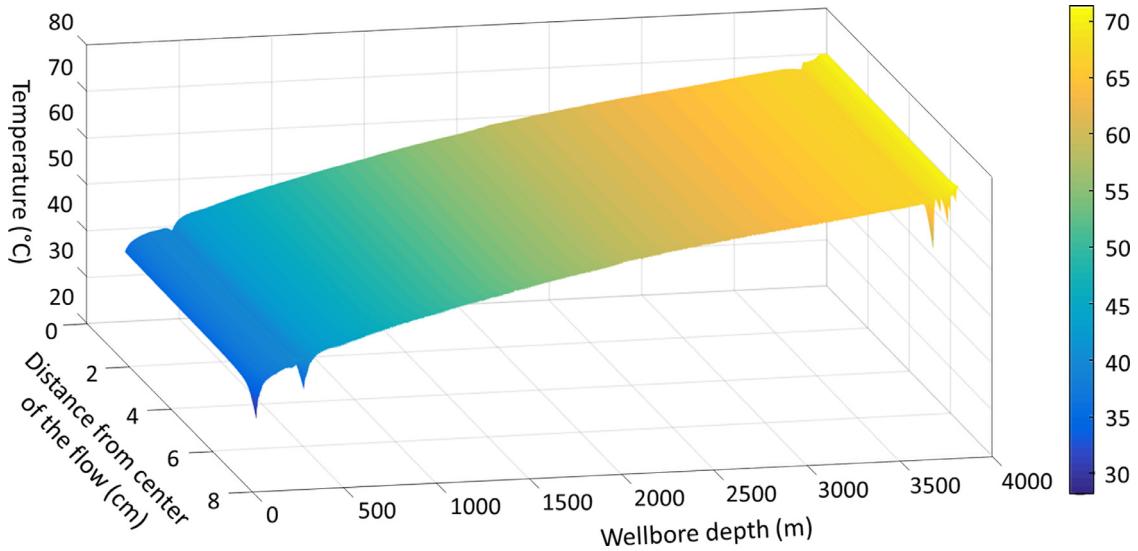

Fig. 2. Results of temperature simulation inside of tubing.

3. Results and discussion

3.1. Validation with PVT properties

The first validations of PC SAFT were performed by comparing PVT properties' predictions of PC SAFT and Peng Robinson EOS. The results are given in Fig. 3.

PC-SAFT shows slightly better accuracy when it comes to Formation Volume Factor predictions even though PR EOS is reasonably accurate. This can be explained due to high accuracy of PC-SAFT compared to PR EoS when it comes to density predictions, especially at high pressure and high temperature. Therefore, Formation Volume Factor which is the ratio of oil volume at reservoir pressure and temperature conditions divided by the oil volume at surface condition can be inaccurate the case of PR EoS. However, Bubble Point Pressure and Gas to Oil Ratio predictions for both models are similar as PR EoS is accurate enough for predictions of gas or oil densities at surface conditions and in case of Bubble Point Pressure.

3.2. Validation on precipitated wax amount

However, due to the unsuitability of the assumption for heavy hydrocarbons, PR EOS cannot properly represent the fugacity of these components in the liquid or gas. Therefore, PC-SAFT was chosen to accomplish this task. The methodology was validated by comparing predictions of the precipitated wax amount at a certain pressure and temperature conditions with the experimental results shared by other authors [27]. Results of PR EoS being applied in Multi Solid and Solution solid formulation can also be found [27]. Our results of PC-SAFT given below in Fig. 4.

Even though having only one precipitating component in composition resulted in a smooth curve of PC-SAFT, the graphs show a reasonable match with experimental data.

3.3. Validation on WAT prediction

As it was explained in the fluid characterization section of this paper, reservoir was divided in the sectors and calibrated separately to be able to predict new well. Therefore, after comparing predictions of the model with the experimental data from literature, WAT predictions were validated by comparing model results with experimental WAT measurements of 3 new wells from different sectors of the field in South Caspian Basin (later referred to as X field). The graphs are given in Fig. 5.

Table 1
Numerical values of the graph in Fig. 5.

	Actual WAT,°C	Predicted WAT,°C	Relative error, %
Well from group 1	42	41.4	1.4
Well from group 2	39	39.5	1.3
Well from group 3	30	29	3.3

Results of Fig. 5 are provided in the Table 1.

All the input parameters of PC-SAFT used during these predictions are provided in Appendix C.

As can be seen from the graphs in Fig. 5, WAT is predicted by PC-SAFT with high accuracy. Moreover, these results were obtained with just a little calibration from properties obtained during PVT modeling. PC-SAFT parameters of wax component obtained from calibration of data from literature [27] was used to start the calibration for every group of wells in our field.

3.4. Sensitivity analysis

In order to identify what affects wax precipitation the most, sensitivity analyses on such parameters as Gas to Oil Ratio, Pressure, and Temperature were carried out. These three sensitivity analyses are illustrated in Fig. 6.

One of the wells that had the average amount of precipitated wax was chosen for sensitivity analysis. In all of these graphs, the red point represents the real condition of the well and blue points are simulated with a changed value of some parameter (GOR, P or T). The X-axis shows how much value chosen for simulation is different from the real one and Y-axis shows how much precipitated amount of wax is changed in that case.

As a conclusion from Fig. 6, the effect of GOR on the amount of precipitated wax was the lowest and it can be considered negligible. The effect of pressure is small compared to temperature; however, at higher pressures the amount of precipitated wax increases by up to 12%. As it was expected, a distinctly dominant parameter is temperature which depending on temperature drop may increase the amount of precipitated wax by 2–4 times

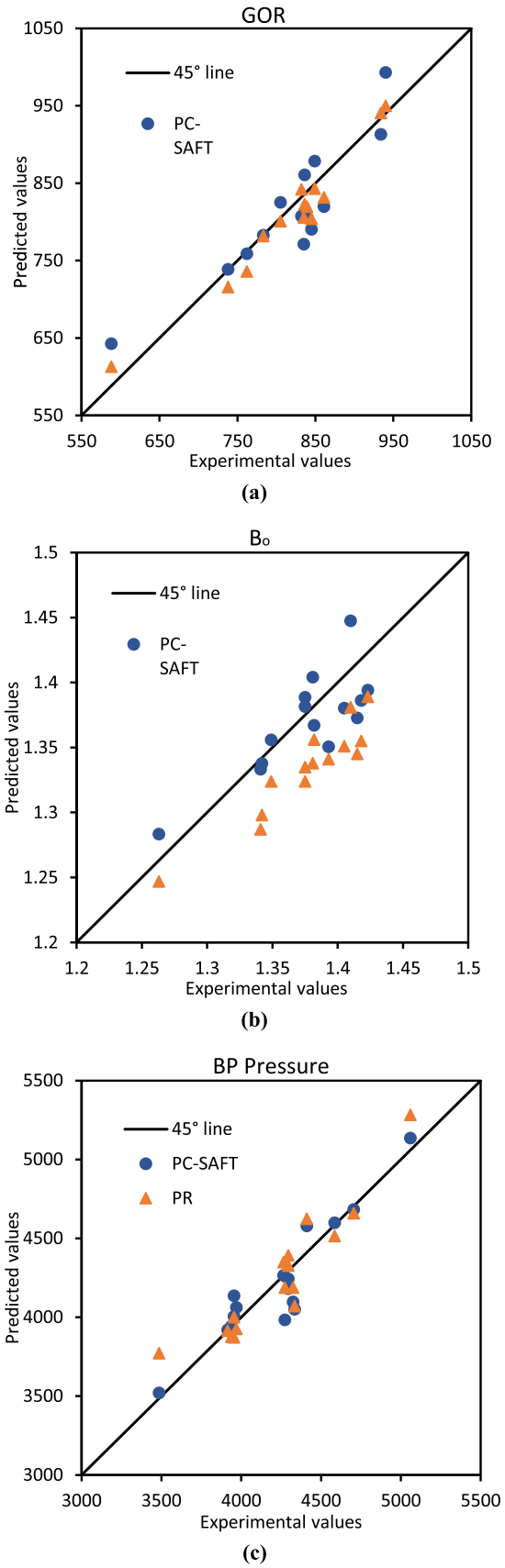

Fig. 3. Comparison of PC-SAFT and Peng Robinson PVT properties predictions on 45° scatter plot, (a) Gas to oil ratio, (b) Formation volume factor of oil, (c) Bubble point pressure.

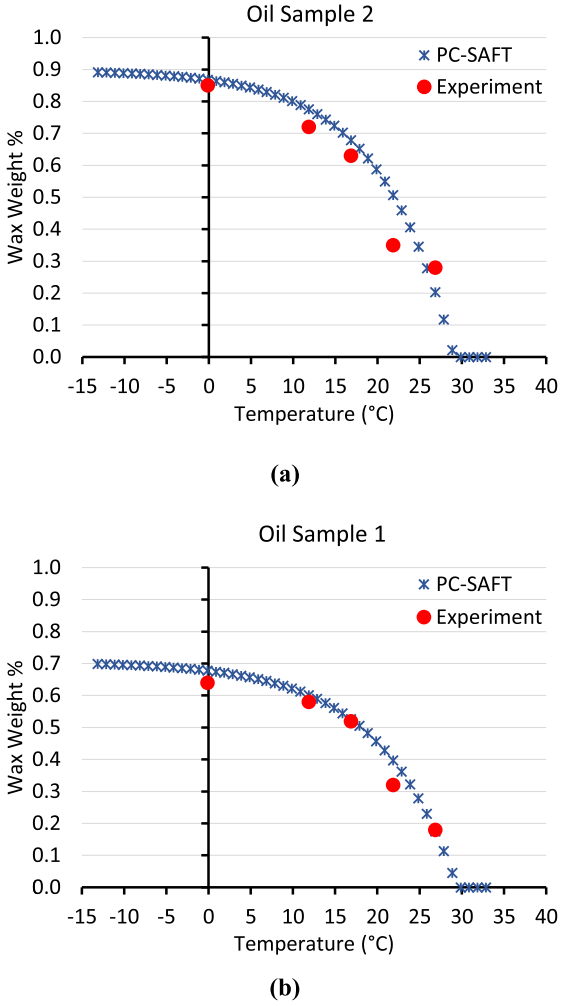

Fig. 4. Precipitated wax weight percentage prediction of PC-SAFT, (a) and (b) are two different oil samples [27].

3.5. Calibration results

Despite the great variations in the composition of oil across the field, it was not attainable to perform compositional analysis for each well. Therefore, during the calibration procedure, the X field was divided into several groups according to geological parameters (location, depth, tilting angle and penetrated layer) each of which contained several wells with experimental data of wax weight percentage and WAT. Then, each of the groups was calibrated separately and a set of parameters were tuned to match experimental WAT.

Results of the calibration procedure is given in Fig. 7 as a plot of WAT predicted for all wells from one group vs wax weight percentage.

Conclusions

Following conclusions can be made out of this study:

- PC-SAFT EOS was implemented in 2 phase and 3 phase flash calculations to model PVT properties and wax precipitation respectively.
- The model was validated by comparing with experimental PVT properties data and PR predictions.

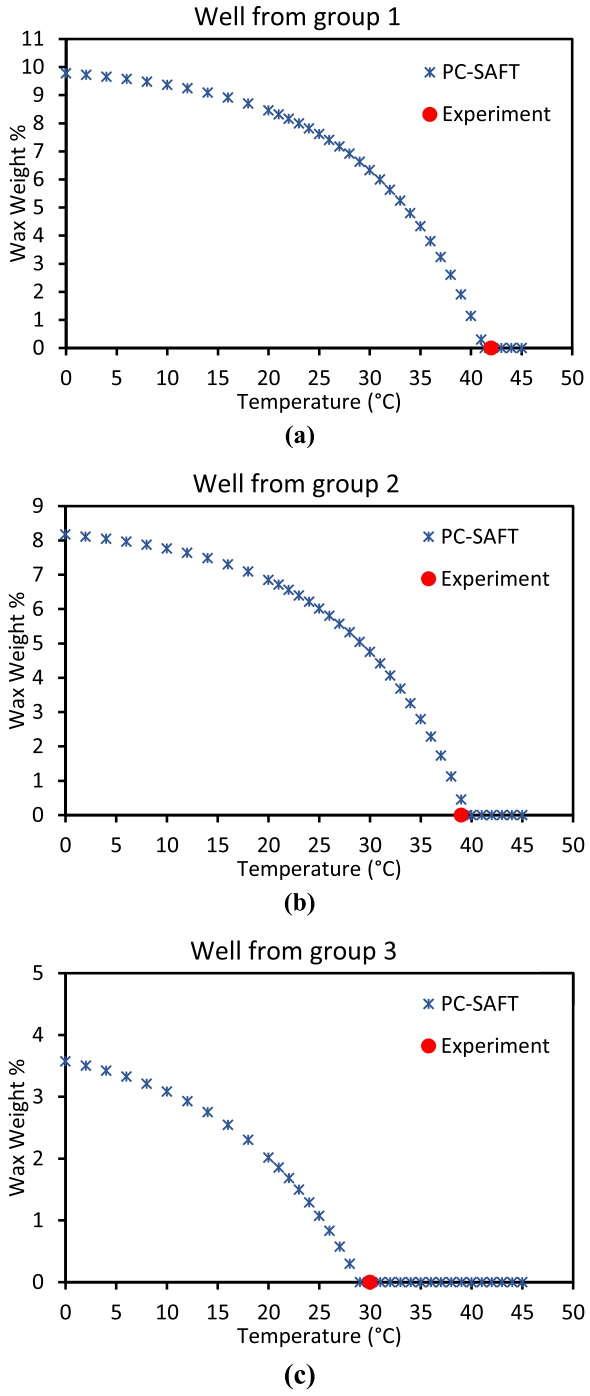

Fig. 5. WAT prediction of PC-SAFT, (a), (b) and (c) are three different wells from different sectors of X field.

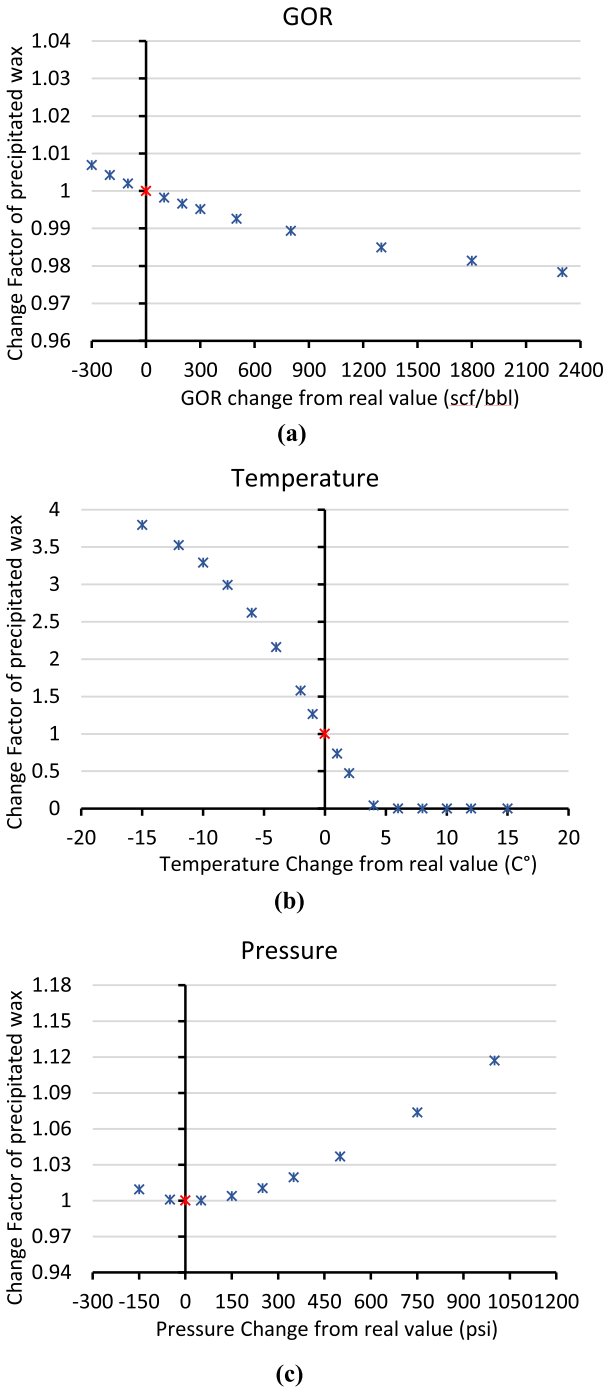

Fig. 6. Sensitivity analysis on (a) Gas Oil Ratio, (b) Pressure, (c) Temperature.

- PC-SAFT model prediction of wax precipitation was compared to experimental values of precipitated wax weight% obtained from research papers and it was also compared to experimental WAT data from the wells located in the South Caspian Basin.
- Sensitivity analysis was performed over a wide range of parameter (GOR, P, T) values. The effect of pressure on wax precipitation was higher at higher pressures; however, the effect of changing GOR and low pressures was almost negligible. As was expected the effect of temperature can result in as high as 4 times increase in wax precipitation.
- The algorithm was written in Python programming language so that it can be easily integrated into the database used by the consortium. Scorecard was created that clearly emphasizes well with high risk of wax precipitation.
- The heat flow equation was applied to determine radial temperature change from tubing wellbore to the flow center as the main source of temperature was DTS which location is outside of the tubing.
- X field was divided into groups according to geological features as true vertical depth, location and penetrated layer. Calibration procedure was performed for each of the groups using the Gradient Descent optimization algorithm and a new, tuned set of parameters were generated for future modeling.

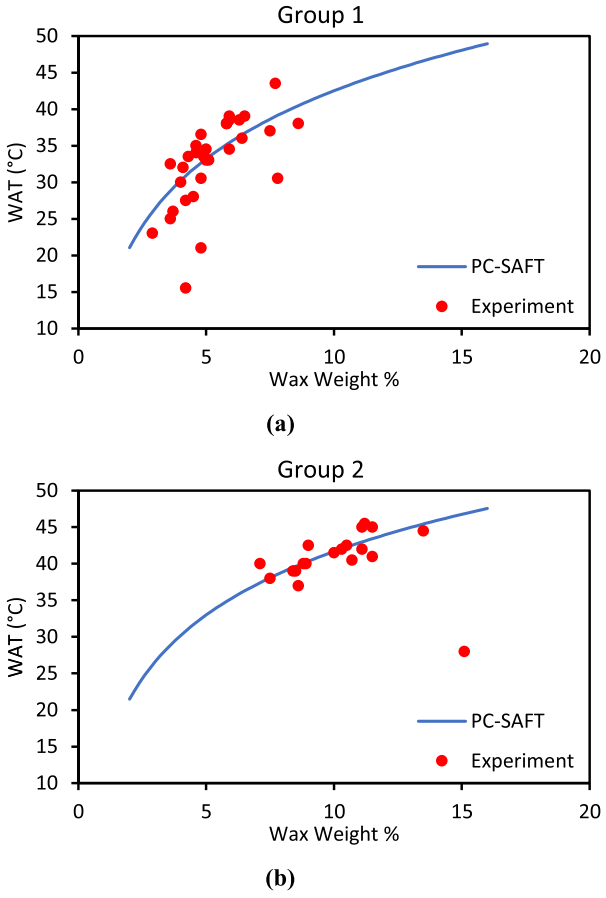

Fig. 7. WAT prediction after calibration.

Declaration of Competing Interest

The authors declare that they have no known competing financial interests or personal relationships that could have appeared to influence the work reported in this paper.

CRediT authorship contribution statement

I. Shahsenov: Methodology, Investigation, Supervision, Writing - review & editing. **I. Baghishov:** Methodology, Investigation, Writing - original draft. **P. Allahverdiyev:** Data curation, Validation, Resources, Writing - review & editing. **E. Azizov:** Project administration, Resources, Validation, Writing - review & editing.

Acknowledgments

This work was supported by the Science Development Foundation under the President of the Republic of Azerbaijan – Grant № EIF-KETPL-2-2015-1(25)-56/08/1-M-21. The authors are grateful to Azerbaijan International Operating Company (AIOC) for providing the data and for the permission to publish the results.

Appendix A

Fig. A1

Appendix B

In order to calculate the fugacity of a component in liquid or vapor mixture using PC-SAFT, density has to be defined. Therefore, as it was shown in Fig. A.1, Newton Raphson method was used to determine density iteratively by adjusting reduced density η until calculated and real pressures converge. A suitable initial value for the reduced density of liquid 0.5 and 10^{-10} for a vapor. Values of η higher than 0.7405 which is the closest packing of segments had no physical meaning. Equations required for calculation of pressure from reduced density when other input parameters are temperature and composition are described as follows.

Pressure calculation from PC-SAFT

Pressure can be calculated using the following relation:

$$P = ZkT\rho\left(10^{10}\frac{A}{m}\right)^3 \tag{A1}$$

Where k is the Boltzmann constant, T is temperature, ρ is number density which calculated from η using eq. (A.2), Z is a compressibility factor.

$$\rho = \frac{6}{\pi}\eta\left(\sum_i x_i m_i d_i^3\right)^{-1} \tag{A2}$$

Where, x_i is a composition of component i, m_i is the number of segments in i component (one of three input parameters of PC-SAFT) and $d_i$is the temperature-dependent segment diameter which is calculated using this formula:

$$d_i(T) = \sigma_i\left[1 - 0.12\exp\left(-\frac{3\varepsilon_i}{kT}\right)\right] \tag{A3}$$

Where, σ_i and ε_i/k are the temperature-independent segment diameters and the depth of the potential well divided by Boltzmann constant respectively which are the remaining two input parameters of PC-SAFT.

After η is adjusted in the Newton Raphson method, molar density $\hat{\rho}$ in units of kmol/m^3 can be determined from number density ρ calculated from Eq. (A.2):

$$\hat{\rho} = \frac{\rho}{N_{AV}}\left(10^{10}\frac{A}{m}\right)^3\left(10^{-3}\frac{kmol}{mol}\right) \tag{A4}$$

Meanwhile, the compressibility factor Z required in Eq. (A.1) is calculated from

$$Z = 1 + Z^{hc} + Z^{disp} \tag{A5}$$

The superscripts *hc* and *disp* denote the hard-chain and dispersion. The calculation of hard-chain contribution to the compressibility factor will be examined separately from dispersion contribution.

The hard-chain contribution

The hard-chain term of the compressibility factor is given by

$$Z^{hc} = \bar{m}Z^{hs} - \sum_i x_i(m_i - 1)\left(g_{ii}^{hs}\right)^{-1}\rho\frac{\partial g_{ii}^{hs}}{\partial\rho} \tag{A6}$$

Where,

$$\bar{m} = \sum_{i=1}^{N_c} x_i m_i \tag{A.7}$$

contribution of hard-sphere to compressibility,

$$Z^{hs} = \frac{\xi_3}{(1-\xi_3)} + \frac{3\xi_1\xi_2}{\xi_0(1-\xi_3)^2} + \frac{3\xi_2^3 - \xi_3\xi_2^3}{\xi_0(1-\xi_3)^3} \tag{A.8}$$

The radial distribution function is expressed as

$$g_{ij}^{hs} = \frac{1}{(1-\xi_3)^2} + \left(\frac{d_i d_j}{d_i + d_j}\right)\frac{3\xi_2}{(1-\xi_3)^2} + \left(\frac{d_i d_j}{d_i + d_j}\right)^2\frac{3\xi_2^3}{(1-\xi_3)^3} \quad for\ i, j = 1, \ldots, N_c \tag{A.9}$$

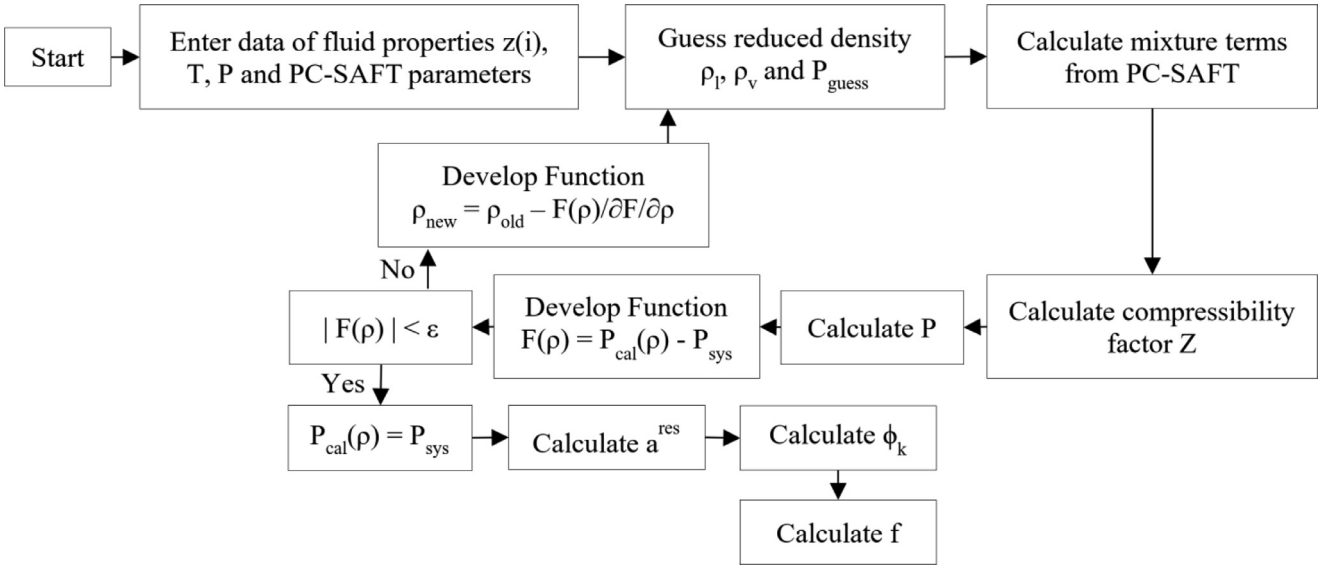

Fig. A.1. Block diagram of calculating fugacity using PC-SAFT.

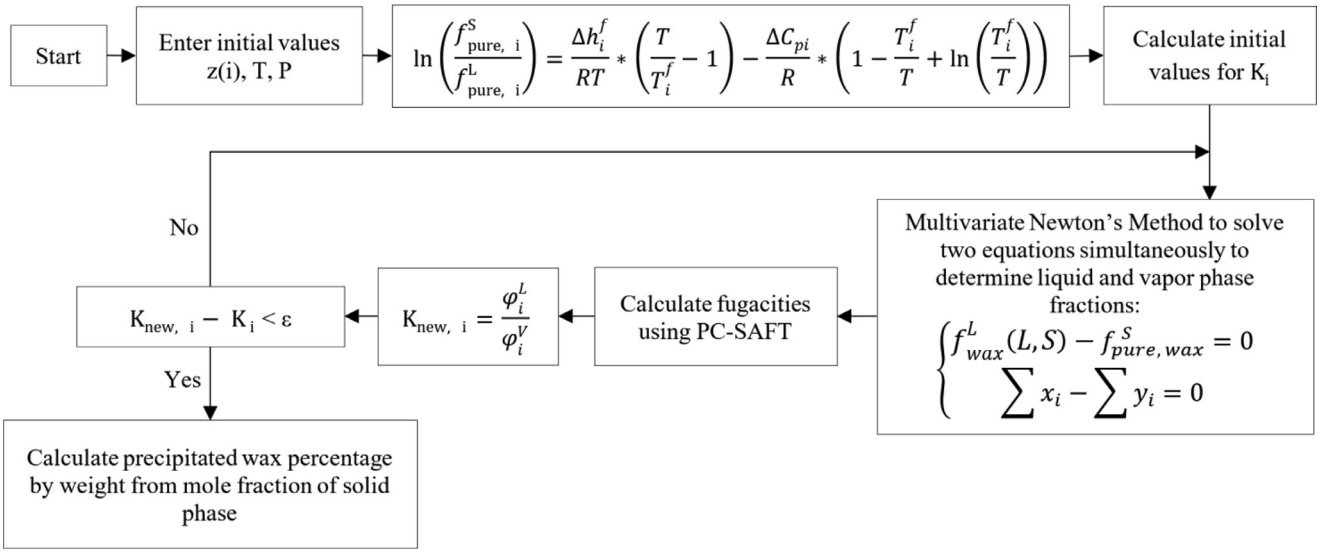

Fig. A.2. Block diagram of Three Phase flash calculation.

and

$$\rho\frac{\partial g_{ii}^{hs}}{\partial\rho}=\frac{\xi_3}{(1-\xi_3)^2}+\frac{d_i}{2}\left(\frac{3\xi_2}{(1-\xi_3)^2}+\frac{6\xi_2\xi_3}{(1-\xi_3)^3}\right)+\frac{d_i^2}{2}\left(\frac{4\xi_2{}^2}{(1-\xi_3)^3}+\frac{6\xi_2^2\xi_3}{(1-\xi_3)^4}\right) \tag{A10}$$

ξ_n is defined as

$$\xi_n=\frac{\pi}{6}\rho\sum_{i=1}^{N_c}x_i m_i d_i^n \quad for\ n=0,\ 1,\ 2,\ 3 \tag{A11}$$

The dispersion contribution

The dispersion contribution to the compressibility factor is given by

$$Z^{disp}=-2\pi\rho\frac{\partial(\eta I_1)}{\partial\eta}\overline{m^2\varepsilon\sigma^3}-\pi\rho\bar{m}\left[C_1\frac{\partial(\eta I_2)}{\partial\eta}+C_2\eta I_2\right]\overline{m^2\varepsilon^3\sigma^3} \tag{A12}$$

Where the abbreviation C_2 is defined as

$$C_2=\frac{\partial C_1}{\partial\eta}=-C_1^2\left[\bar{m}\frac{-4\eta^2+20\eta+8}{(1-\eta)^5}+(1-\bar{m})\frac{2\eta^3+12\eta^2-48\eta+40}{(1-\eta)^3(2-\eta)^3}\right] \tag{A14}$$

Where, C_1, $\overline{m^2\varepsilon\sigma^3}$, and $\overline{m^2\varepsilon^2\sigma^3}$are calculated from

$$C_1=\left(1+m\frac{8\eta-2\eta^2}{(1-\eta)^4}+(1-m)\frac{20\eta-27\eta^2+12\eta^3-2\eta^4}{[(1-\eta)(2-\eta)]^2}\right)^{-1} \tag{A15}$$

$$\overline{m^2\varepsilon\sigma^3}=\sum_{i=1}^{N_c}\sum_{j=1}^{N_c}x_i x_j m_i m_j\left(\frac{\varepsilon_{ij}}{kT}\right)\sigma_{ij}^3 \tag{A16}$$

$$\overline{m^2\varepsilon^2\sigma^3}=\sum_{i=1}^{N_c}\sum_{j=1}^{N_c}x_i x_j m_i m_j\left(\frac{\varepsilon_{ij}}{kT}\right)^2\sigma_{ij}^3 \tag{A17}$$

The parameters for a pair of unlike segments, ε_{ij} and σ_{ij}, are determined by

$$\varepsilon_{ij} = \sqrt{\varepsilon_i \varepsilon_j}\left(1 - k_{ij}\right) \tag{A18}$$

$$\sigma_{ij} = \frac{1}{2}\left(\sigma_i + \sigma_j\right) \tag{A19}$$

Where $k_{ij}$is a binary interaction parameter (BIP) between components i and j.

The terms $I_1$and I_2 are the integrals defined by the perturbation theory, which can be simplified to two simple power series as follows:

$$I_1(\eta, \bar{m}) = \sum_{i=0}^{6} a_i(\bar{m})\eta^i \tag{A.20}$$

$$I_2(\eta, \bar{m}) = \sum_{i=0}^{6} b_i(\bar{m})\eta^i \tag{A.21}$$

Partial derivatives used n eq. (A.12) are defined from,

$$\frac{\partial(\eta I_1)}{\partial \eta} = \sum_{i=0}^{6} a_i(\bar{m})(i+1)\eta^i \tag{A.22}$$

$$\frac{\partial(\eta I_2)}{\partial \eta} = \sum_{i=0}^{6} b_i(\bar{m})(i+1)\eta^i \tag{A.23}$$

and the a_i and b_i are related to the chain length by the following equations:

$$a_i(\bar{m}) = a_{i0} + \left(\frac{\bar{m}-1}{\bar{m}}\right)a_{1i} + \left(\frac{\bar{m}-1}{\bar{m}}\right)\left(\frac{\bar{m}-2}{\bar{m}}\right)a_{2i} \tag{A.24}$$

and

$$b_i(\bar{m}) = b_{i0} + \left(\frac{\bar{m}-1}{\bar{m}}\right)b_{1i} + \left(\frac{\bar{m}-1}{\bar{m}}\right)\left(\frac{\bar{m}-2}{\bar{m}}\right)b_{2i} \tag{A.25}$$

The model constants a_{i0}, a_{1i}, a_{2i}, b_{i0}, b_{1i}, and $b_{2i}$are presented in Table A-1 and Table A-2.

Fugacity calculation

Now, in order to calculate the fugacity of any component, it is required to calculate the fugacity coefficient from PC-SAFT and multiply it by the pressure of the system. Fugacity coefficient $\varphi_k(T, P)$ is related to the residual chemical potential as

$$ln\varphi_k = \frac{\mu_k^{res}(T, v)}{kT} - \ln Z \tag{A.26}$$

The chemical potential can be obtained from

$$\frac{\mu_k^{res}(T, v)}{kT} = \tilde{a}^{res} + (Z-1) + \left(\frac{\partial \tilde{a}^{res}}{\partial X_k}\right)_{T,V,X_{i\neq k}} - \sum_{j=1}^{N}\left[X_j\left(\frac{\partial \tilde{a}^{res}}{\partial X_k}\right)_{T,V,X_{i\neq j}}\right] \tag{A.27}$$

Where, $\tilde{a}^{res}$ is the reduced Helmholtz free energy defined as

$$\tilde{a}^{res} = \tilde{a}^{hc} + \tilde{a}^{disp} \tag{A.28}$$

Where dispersion contribution to residual Helmholtz free energy defined as,

$$\tilde{a}^{disp} = -2\pi\rho I_1(\rho, \bar{m})\overline{m^2\varepsilon\sigma^3} - \pi\rho\bar{m}C_1 I_2(\rho, \bar{m})\overline{m^2\varepsilon^2\sigma^3} \tag{A.29}$$

and hard chain contribution determined from

$$\tilde{a}^{hc} = \bar{m}\tilde{a}^{hs} - \sum_{i=1}^{N_c} x_i(m_i - 1)lng_{ii}^{hs}(d_{ii}) \tag{A.30}$$

Where the hard-sphere contribution is

$$\tilde{a}^{hs} = \frac{1}{\xi_0}\left[\frac{3\xi_1\xi_2}{(1-\xi_3)} + \frac{\xi_2^3}{\xi_3(1-\xi_3)^2} + \left(\frac{\xi_2^3}{\xi_3^2}\right)\ln(1-\xi_3)\right] \tag{A.31}$$

Derivatives in Eq. (A.27) with respect to mole fractions are calculated regardless of the summation relation $\sum_j X_j = 1$ For convenience, one can define abbreviations for derivatives of Eq (A.11) with respect to mole fraction.

$$\xi_{n,\,xk} = \left(\frac{\partial \xi_n}{\partial X_k}\right)_{T,\rho,X_{j\neq k}} = \frac{\pi}{6}\rho m_k (d_k)^n \quad n \in \{0,\ 1,\ 2,\ 3\} \tag{A.32}$$

Hard-Chain Reference Contribution.

$$\left(\frac{\partial \tilde{a}^{hc}}{\partial X_k}\right)_{T,\rho,X_{j\neq k}} = m_k\tilde{a}^{hs} + \bar{m}\left(\frac{\partial \tilde{a}^{hs}}{\partial X_k}\right)_{T,\rho,X_{j\neq k}} - \sum_i x_i(m_i - 1)\left(g_{ii}^{hs}\right)^{-1}\left(\frac{\partial g_{ii}^{hs}}{\partial X_k}\right)_{T,\rho,X_{j\neq k}} \tag{A.33}$$

With

$$\left(\frac{\partial \tilde{a}^{hs}}{\partial X_k}\right)_{T,\rho,X_{j\neq k}} = -\frac{\xi_{0,xk}}{\xi_0}\tilde{a}^{hs} + \frac{1}{\xi_0}\left[\frac{3\left(\xi_{1,xk}\xi_2 + \xi_1\xi_{2,xk}\right)}{(1-\xi_3)} + \frac{3\xi_1\xi_2\xi_{3,xk}}{(1-\xi_3)^2} + \frac{3\xi_2^2\xi_{2,xk}}{\xi_3(1-\xi_3)^2} + \frac{\xi_2^3\xi_{3,xk}(3\xi_3 - 1)}{\xi_3^2(1-\xi_3)^3} + \left(\frac{3\xi_2^2\xi_{2,xk}\xi_3 - 2\xi_2^3\xi_{3,xk}}{\xi_3^3} - \xi_{0,xk}\right)\ln(1-\xi_3) + \left(\xi_0 - \frac{\xi_2^3}{\xi_3^2}\right)\frac{\xi_{3,xk}}{(1-\xi_3)}\right] \tag{A.34}$$

$$\left(\frac{\partial g_{ij}^{hs}}{\partial X_k}\right)_{T,\rho,X_{j\neq k}} = \frac{\xi_{3,xk}}{(1-\xi_3)^2} + \left(\frac{d_i d_j}{d_i + d_j}\right)\left(\frac{3\xi_{2,xk}}{(1-\xi_3)^2} + \frac{6\xi_2\xi_{3,xk}}{(1-\xi_3)^3}\right) + \left(\frac{d_i d_j}{d_i + d_j}\right)^2\left(\frac{4\xi_2\xi_{2,xk}}{(1-\xi_3)^3} + \frac{6\xi_2^2\xi_{3,xk}}{(1-\xi_3)^4}\right) \tag{A.35}$$

Dispersion Contribution.

$$\left(\frac{\partial \tilde{a}^{hs}}{\partial X_k}\right)_{T,\rho,X_{j\neq k}} = -2\pi\rho\left[I_{1,xk}\overline{m^2\epsilon\sigma^3} + I_1\left(\overline{m^2\epsilon\sigma^3}\right)_{xk}\right] - \pi\rho\left\{\left[m_k C_1 I_2 + \bar{m}C_{1,xk}I_2 + \bar{m}C_1 I_{2,xk}\right]\overline{m^2\epsilon^2\sigma^3} + \bar{m}C_1 I_2\left(\overline{m^2\epsilon^2\sigma^3}\right)_{xk}\right\} \tag{A.36}$$

With

$$\left(\overline{m^2\epsilon\sigma^3}\right)_{xk} = 2m_k\sum_j x_j m_j\left(\frac{\epsilon_{kj}}{kT}\right)\sigma_{kj}^3 \tag{A.37}$$

$$\left(\overline{m^2\epsilon^2\sigma^3}\right)_{xk} = 2m_k\sum_j x_j m_j\left(\frac{\epsilon_{kj}}{kT}\right)^2\sigma_{kj}^3 \tag{A.38}$$

$$C_{1,xk} = C_2\xi_{3,xk} - C_1^2\left\{m_k\frac{8\eta - 2\eta^2}{(1-\eta)^4} - m_k\frac{20\eta - 27\eta^2 + 12\eta^3 - 2\eta^4}{[(1-\eta)(2-\eta)]^2}\right\} \tag{A.39}$$

$$I_{1,xk} = \sum_{i=0}^{6}\left[a_i(\bar{m})i\xi_{3,xk}\eta^{i-1} + a_{i,xk}\eta^i\right] \tag{A.40}$$

$$I_{2,xk} = \sum_{i=0}^{6}\left[b_i(\bar{m})i\xi_{3,xk}\eta^{i-1} + b_{i,xk}\eta^i\right] \tag{A.41}$$

$$a_{i,xk} = \frac{m_k}{\bar{m}^2} a_{1i} + \frac{m_k}{\bar{m}^2}\left(3 - \frac{4}{\bar{m}}\right) a_{2i} \quad \text{(A.42)}$$

$$b_{i,xk} = \frac{m_k}{\bar{m}^2} b_{1i} + \frac{m_k}{\bar{m}^2}\left(3 - \frac{4}{\bar{m}}\right) b_{2i} \quad \text{(A.43)}$$

Table A.5
Tuned Parameters for simulating WAT (Fig. 5).

	Well 1	Well2	Well 3
m_i	9.4823	9.4802	9.4909
σ_i	4.0346	4.0487	4.1202
ε_i/k	319.9814	319.9804	319.9766
T^f_{wax}	349.9885	349.9883	354.9891
Δh^f_{wax}	16999.9994	16999.9996	16999.9996

Appendix C

Table A.1
Universal constants for Eq. (A.24) [4].

i	a_{i0}	a_{1i}	a_{2i}
0	0.91056314452	-0.30840169183	-0.09061483510
1	0.63612814495	0.18605311592	0.45278428064
2	2.68613478914	-2.50300472587	0.59627007280
3	-26.5473624915	21.4197936297	-1.72418291312
4	97.7592087835	-65.2558853304	-4.13021125312
5	-159.591540866	83.3186804809	13.7766318697
6	91.2977740839	-33.7469229297	-8.67284703680

Table A.2
Universal constants for Eq. (A.25) [4].

i	b_{i0}	b_{1i}	b_{2i}
0	0.72409469413	-0.57554980753	0.09768831158
1	2.23827918609	0.69950955214	-0.25575749816
2	-4.00258494846	3.89256733895	-9.15585615297
3	-21.0035768149	-17.2154716478	20.6420759744
4	26.8556413627	192.672264465	-38.8044300521
5	206.551338407	-161.826461649	93.6267740770
6	-355.602356122	-165.207693456	-29.6669055852

Table A.3
Binary interaction coefficients

	CO2	C1-N2	C2	C3-C4	C5-C10	C11-C20	C21+	wax
CO2	0							
C1-N2	0.049311	0						
C2	0.099312	0	0					
C3-C4	0.099311	0	0	0				
C5-C10	0.129308	0.028762	0.009812	0.009729	0			
C11-C20	0.099302	0.098071	0.009789	0.009715	0.00555	0		
C21+	0.099303	0.027427	0.009793	0.009705	0.002539	0.001658	0	
Wax	0.099303	0.09	0.009793	0.009705	0.006	0.001658	0.0005	0

Table A.4
Input parameters for simulating WAT (Fig. 5).

	PC-SAFT parameters				Composition (%)		
	MW	m_i	σ_i	ε_i/k	Well 1	Well 2	Well 3
CO2	44.01	2.0729	2.7852	169.21	0	0	0
C1-N2	16.062	1	3.7039	150.03	0	0	0
C2	30.07	1.6069	3.5206	191.42	0.07	0.19	0
C3-C4	50.616	2.1668	3.6635	215.495	3.53	1.11	2.28
C5-C10	104.35	3.654346	3.87076287	239.586646	49.88	43.81	51.42
C11-C20	203.812	6.47872755	3.87599111	263.630334	35.43	35.61	36.39
C21+	421.001	8.3659206	4.08056531	293.656297	6.76	15.05	8.21
wax	400	given in Table A.4			4.34	4.23	1.70

References

[1] Sanjay, M., Simanta, B., & Kulwant, S., Paraffin problems in crude oil production and transportation: a review. (1995, February 1).
[2] K.W. Won, Continuous thermodynamics for solid-liquid equilibria: wax formation from heavy hydrocarbon mixtures, Fluid Phase Equilib. 30 (1986) 265–279.
[3] K.W. Won, Thermodynamic calculation of cloud point temperatures and wax phase compositions of refined hydrocarbon mixtures, Fluid Phase Equilib. 53 (1989) 377–396.
[4] J.H. Hansen, A. Fredenslund, K.S. Pedersen, H.P. Ronningsen, A thermodynamic model for predicting wax formation in crude oils, AIChE J. 34 (1988) 1937–1942.
[5] P.J. Flory, Thermodynamics of high polymer solutions, J. Chem. Phys. 9 (1941) 660–661.
[6] K.S. Pedersen, P. Skovborg, H.P. Ronningsen, Wax precipitation from North Sea crude oils. 4, Thermodyn. Model. Energy Fuels 5 (1991) 924–932.
[7] J.A.P. Coutinho, E.H. Stenby, Predictive local composition models for solid/liquid equilibrium in n-alkane systems: Wilson equation for multicomponent systems, Ind. Eng. Chem. Res. 35 (1996) 918–925 vol pp.
[8] J.A.P. Coutinho, Predictive UNIQUAC: a new model for the description of multiphase solid-liquid equilibria in complex hydrocarbon mixtures, Ind. Eng. Chem. Res. 37 (1998) 4870–4875.
[9] J.Y. Zuo, D.D. Zhang, H.-J. Ng, An improved thermodynamic model for wax precipitation from petroleum fluids, Chem. Eng. Sci. 56 (2001) 6941–6947.
[10] H.Y. Ji, B. Tohidi, A. Danesh, A.C. Todd, Wax phase equilibria: developing a thermodynamic model using a systematic approach, Fluid Phase Equilib. 216 (2004) 201–217.
[11] F. Esmaeilzadeh, J.F. Kaljahi, E. Ghanaei, Investigation of different activity coefficient models in thermodynamic modeling of wax precipitation, Fluid Phase Equilib. 248 (2006) 7–18.
[12] J.A.P. Coutinho, V. Ruffier-Meŕay, Experimental measurements and thermodynamic modeling of paraffinic wax formation in undercooled solutions, Ind. Eng. Chem. Res. 36 (1997) 4977–4983.
[13] C. Lira-Galeana, A. Firoozabadi, J.M Prausnitz, Thermodynamics of wax precipitation in petroleum mixtures, AIChE J. 42 (1996) 239–248.
[14] M. Vafaie-Sefti, S. A. Mousavi-Dehghani, M. M. Bahar Modification of multi-solid phase model for prediction of wax precipitation: a new and effective solution method Fluid Phase Equilib., 2007, vol. 173, pp. 65–80.
[15] R. Dalirsefat, F. Feyzi, A thermodynamic model for wax deposition phenomena, Fuel 86 (2007) 1402–1408.
[16] J. Gross, G. Sadowski, SAFT Perturbed-chain, an equation of state based on perturbation theory for chain molecules, Ind. Eng. Chem. Res. 40 (2001) 1244–1260.
[17] R Venkatesan, The Deposition and Rheology of Organic gels Ph.D. thesis, University of Michigan, 2004.
[18] M.K. Siljuberg, Modelling of Paraffin Wax in Oil Pipelines Ph.D. thesis, Norwegian University of Science and Technology, 2012.
[19] W.G. Chapman, G. Jackson, K.E. Gubbins, Phase equilibria of associating fluids. Chain molecules with multiple bonding sites, Mol. Phys. c65 (1988) 1057.
[20] Wertheim Fluids with highly directional attractive forces: IV. Equilibrium polymerization, J. Stat. Phys. 42 (1986) 477–482.
[21] J.A. Barker, D. Henderson, Perturbation theory and equation of state for fluids: the square-well potential, J. Chem. Phys. 47 (1967) 2856–2861.
[22] G.A. Mansoori, N.F. Carnahan, K.E. Starling, T.W. Leland, Equilibrium thermodynamic properties of the mixture of hard spheres, J. Chem. Phys. 54 (1971) 1523–1531.
[23] J.M. Prausnitz, R.N. Lichtenthaler, E.G. de Azevedo, Molecular Thermodynamics of Fluid-Phase Equilibria, Third ed., 1999, pp. 638–640.
[24] W. Chen, Z. Zhao, X. Zhang, L. Wang, Thermodynamic phase equilibria of wax precipitation in crude oils, Fluid Phase Equilib. 255 (2007) 31–36.
[25] P.H. Oosthuizen, D. Naylor, Introduction to Convective Heat Transfer Analysis, Mc Graw Hill, 1999.
[26] Hyun Su Lee, Computational and Rheological Study of Wax Deposition and Gelation in Subsea Pipelines Ph.D. thesis, The University of Michigan, 2008.
[27] C. Ghotbi, H. Mashhadi Meighani, T. Jafari Behbahani, A modified thermodynamic modeling of wax precipitation in crude oil based on the PC-SAFT model, Fluid Phase Equilib. 429 (2016) 313–324.